

– 1 –

# Modeling RR Tel through the Evolution of the Spectra

Marcella Contini<sup>1</sup> and Liliana Formiggini<sup>2</sup>

<sup>1</sup> School of Physics and Astronomy, Tel-Aviv University, Ramat-Aviv, Tel-Aviv, 69978, Israel

<sup>2</sup> Wise Observatory, The Raymond and Beverly Sackler Faculty of Exact Sciences, Tel-Aviv University, Tel-Aviv, 69978, Israel

Running title : The evolution of RR Tel

Subject headings: binaries:symbiotic - shock waves - stars: individual: (RR Telescopii)

## Abstract

We investigate the evolution of RR Tel after the outburst by fitting the emission spectra in two epochs. The first one (1978) is characterized by large fluctuations in the light curve and the second one (1993) by the slow fading trend. In the frame of a colliding wind model two shocks are present: the reverse shock propagates in the direction of the white dwarf and the other one expands towards or beyond the giant. The results of our modeling show that in 1993 the expanding shock has overcome the system and is propagating in the nearby ISM. The large fluctuations observed in the 1978 light curve result from line intensity rather than from continuum variation. These variations are explained by fragmentation of matter at the time of head-on collision of the winds from the two stars. A high velocity ( $500 \text{ km s}^{-1}$ ) wind component is revealed from the fit of the SED of the continuum in the X-ray range in 1978, but is quite unobservable in the line profiles. The geometrical thickness of the emitting clumps is the critical parameter which can explain the short time scale variabilities of the spectrum and the trend of slow line intensity decrease.

## 1. Introduction

RR Tel belongs to the group of symbiotic novae. They are distinguished from classic symbiotic stars by having undergone only one single major outburst and have not yet recovered. The outburst of RR Tel started in 1944 when the system brightened by 7 mag. The light curve after the outburst shows a gradual fading which is still in progress. Besides the general decrease, the light curve is marked by periods of large fluctuations. The system is believed to be a binary, consisting of a nuclear burning white dwarf (WD) and a late type companion, and an emission nebula photoionized by the hot star. The cool component is a Mira-type variable, with a pulsation period of 387 days (Feast et al. 1983). Weak TiO absorption bands of spectral type about M5 were observed by Thackeray (1977). The system has been monitored in many different spectral regions, ranging from radio to X-rays, and, recently, was observed by the HST. In spite of being extensively studied (Aller et al 1973, Thackeray 1977, Hayes & Nussbaumer 1986, etc.), many questions about RR Tel remain unsolved.

The emission line spectra of symbiotic stars are usually calculated using a classical model where the main excitation mechanism is photoionization from the hot star (Murset et al 1991). However, in the last few years, the importance of the winds from both components in symbiotic systems and their collision has been addressed by many authors (e.g. Wallerstein et al 1984, Girard & Willson 1987, Nussbaumer & Walder 1993, etc.).

Recently a model has beeen successfully applied to the calculation of the line and continuum spectra of HM Sge (Formiggini, Contini, & Leibowitz 1995) and AG Peg (Contini 1997). This model is able to fit the high and low ionization emission lines by taking into account both the shock created by the winds and the photoionization flux from the hot star.

In this paper we investigate the evolution of RR Tel through the interpretation of both line and continuum spectra in different epochs. Both the photoionizing flux from the hot star and the collision of the winds are considered, therefore the calculation was performed with the SUMA code. SUMA (Contini 1997 and references therein) consistently accounts for both the radiation from the hot star and for the shock in a plane parallel geometry. Dust reradiation is also consistently calculated.

In §2 the evolution of the outburst is described. In §3 the general model is presented. The spectra in 1978 and 1993 are discussed in §4 and §5, respectively. Model results in the

two epochs 1978 and 1993 are compared in §6 and conclusions follow in §7.

## 2. The evolution of the outburst

Fig. 1 shows the visual light curve of RR Tel between the years 1949 and 1995 which was obtained collecting data from various sources (AAVSO circulars, Heck & Manfroid 1985, and Bateson 1995). A period of 387 days was observed (Heck & Manfroid 1982) for the system after 1930, the same which is observable in the infrared (Feast et al 1983). It can be noticed that a general decreasing trend started in 1949 and is still in progress. Above the fading trend the curve displays a decrease slightly larger than 0.5 mag in the years 1962 - 1963 and particularly large fluctuations in the years 1975-1982. During these years the cool companion remained quite stable as shown by many observations collected at infrared wavelengths where the cool star dominates. In fact a periodicity of 387 days has been detected on JHKL photometric data during 1975-1981 by Feast et al (1983). After these events the system recovered the general fading trend.

Penston et al (1983) reported optical photometric variations from night to night and within a single night between 1975 and 1982. We recall that the line spectrum is very rich, and that some strong lines fall in the passbands of the broad band photometry. It is then likely that large fluctuations in the line intensities are the source of the strong variations in the visual light curve. However, the question of whether the variation in the continuum or in the line intensities are the cause of the photometric fluctuations, is still open.

The outburst event led initially to an extended atmosphere around the white dwarf. The nebular phase emerged some years later and is characterized by a wind with a terminal velocity increasing from  $400 \text{ km s}^{-1}$  in 1949 to  $1300 \text{ km s}^{-1}$  in 1960 (Thackeray 1977). However, when IUE became operational in 1978 Penston et al (1983) measured a terminal velocity of about  $75 \text{ km s}^{-1}$ , indicating that the wind had decelerated from initial velocities of thousands of  $\text{km s}^{-1}$  to less than  $100 \text{ km s}^{-1}$ .

As the outburst evolved, emission lines from high ionization levels appeared (Viotti 1988). The emission line spectra of RR Tel were studied by Penston et al (1983), Hayes & Nussbaumer (1986), Aufdenberg (1993), etc. Recently Zuccolo, Selvelli, & Hack(1997) (from hereafter ZSH) retrieved all the available IUE spectra up to 1993 and after an accurate

reduction and correction for spectral artifacts, saturation and other instrumental effects, a homogenous and complete list of the emission lines in the UV range was presented.

ZSH claim that the variations observed in the emission line intensities from 1978 to 1993 show a rather strong correlation with the line ionization level. The decrease is by a factor larger than 3 and up to 10 for low ionization lines and between 2 and 3 for medium and high ionization lines. The fluxes for some representative lines from ZSH Table 1, are plotted in Fig. 2. It can be noticed that among the high ionization level lines, only [MgVI] 1806 has increased between 1983 and 1993. It seems that the conditions of the system did not change significantly. Hayes & Nussbaumer (1986) already noticed a lack of periodic variation in the UV line fluxes over the period 1978-1984, finding only a slight decrease of the intensities. A modulation of the line intensities with orbital phase is observed in symbiotic stars (e.g. Kenyon et al 1993 for AG Peg). The lack of periodicity of the RR Tel line intensities over a 15 years span (1978-1993) can be explained either by the system being face-on or by a period longer than 15 y. Orbital periods of symbiotic Miras are believed to be longer than 20 years (Withelock 1988).

Actually, for the modeling purpose, we consider the system in two representative epochs, one in 1978 when the system underwent high variability in the visual light on small time scale, and the other in 1993 after recovering the slow fading trend. We take advantage of the ZSH collection of data for the fitting of model calculations.

### 3. The general model

A description of the colliding wind model is given by Girard & Willson (1987). Recall that the cool component of RR Tel is a Mira, characterized by a strong mass loss rate that produces an extended atmosphere. The outburst is the starting point of the wind from the hot star. The winds from the two components approach from opposite directions and collide head-on in the region between the stars and head-on-tail outside. It is plausible that fragmentation of matter in geometrically thin clumps results from turbulence caused by collision. The WD ejecta propagate in the giant atmosphere towards higher densities. Due to the collision two main shocks appear, the reverse shock and the expanding one. The reverse shock propagates back in the WD ejecta facing the WD. Therefore, the photoionizing radiation flux from the WD reaches the very shock front. On the other hand,

the secondary shock expanding towards the red giant, propagates in a denser medium, therefore, its velocity is lower than that of the reverse one. In this case the radiation from the WD reaches the matter downstream, opposite to the shock front. A simple sketch of the model in different epochs is given in Figs. 3a and 3b.

The initially high velocity of the WD wind will produce high densities and temperatures behind the shock front, and hence hard X-ray emission would be expected. However, after propagating and sweeping up additional material the shock decelerates. Lower shock velocities correspond to lower temperatures downstream and the ionized region behind the shock front will become visible in the UV and optical spectra. In our model of RR Tel two gas regions contribute to the emission spectra : downstream of the reverse shock and downstream of the expanding one.

In this paper we consider the system in the two epochs 1978 and in 1993. The input parameters for the calculation of the emitted spectra by SUMA are the following : the shock velocity,  $V_s$ ; the preshock density,  $n_0$ ; the magnetic field,  $B_0$ ; the colour temperature of the hot star,  $T_*$ ; the ionization parameter,  $U$ ; the relative abundances of the elements; and  $d/g$ , the dust-to-gas ratio by number. The models are matter bound and the geometrical thickness of the emitting clumps,  $d$ , is defined by the best results.

The choice of the input parameters is based on the observational evidence at the epochs selected for modeling. The densities are constrained by the critical line ratios (Nussbaumer & Schild, 1981) and the shock velocities by the FWHM of the line profiles. For all models  $T_* = 1.4 \times 10^5$  K (Murset et al. 1991) and  $B_0 = 10^{-3}$  gauss, which is suitable to red giant atmospheres (Bohigas et al 1989), are adopted. Relative abundances are calculated phenomenologically within the range of values which are consistent with CV systems.

#### 4. The spectra in 1978

The models which best fit the observation data are selected from a grid of model calculations. Notice, however, that, whenever different regions of emitting gas coexist in one object, the observed spectrum contains the contribution from all of them. Therefore, although some models better fit high ionization lines and other low ionization lines, the most probable model must consistently account for all the lines and the continuum.

#### 4.1. The line spectrum in the UV

In Table 1 the models are described and in Table 2 the calculated line ratios (to CIV 1533+1548 = 100) are compared with the observed data from ZSH. The arrows indicate that the multiplet is summed up.

FWHM of line profiles from the observations are listed in column 3 of Table 2. Penston et al (1983) measured in 1978 a terminal velocity of the wind of about  $75 \text{ km s}^{-1}$ , indicating that the wind decelerated from initial velocities of thousands of  $\text{km s}^{-1}$  to less than  $100 \text{ km s}^{-1}$ . Large features were actually not observed, however, wide feet of the high level lines are not excluded by Nussbaumer & Dumm (1997) in later spectra.

We consider here the most significative lines. The spectrum at 1978 contains lines from relatively high levels (OV], NV, etc) down to neutral lines. As already noticed by ZSH, the broader the line, the higher the level of the ion. The line widths range between  $70 \text{ km s}^{-1}$  and  $30 \text{ km s}^{-1}$ . The profiles are separated into two groups, one with  $\text{FWHM} \sim 40 \text{ km s}^{-1}$  and the other with  $\text{FWHM}$  up to  $\sim 80 \text{ km s}^{-1}$ . It is known that broad and narrow profiles of single lines characterize most of the symbiotic spectra. In RR Tel the two main widths are very close to each other and difficult to recognize.

Model REV1(Table 1) with a shock velocity of  $80 \text{ km s}^{-1}$  and a density of  $10^6 \text{ cm}^{-3}$  represents the reverse shock. This model nicely fits high ionization lines (from levels higher than III). NIV] 1386 is overestimated by a factor of 4, while [Mg V] 1324 is underestimated, but the identification of this line is doubtful (ZSH). An alternative model for the reverse shock is REV2 characterized by a lower density ( $10^5 \text{ cm}^{-3}$ ), corresponding to a different location of the emitting clump in the system.

Model EXP represents the shock propagating towards the red giant, and is characterized by a velocity of  $45 \text{ km s}^{-1}$  and a density of  $2 \times 10^6 \text{ cm}^{-3}$  as indicated by the observations. The absolute intensity of CIV is extremely low for  $V_s < 50 \text{ km s}^{-1}$  and  $U < 0.01$ , therefore, the line ratios to CIV =100 are very high for this model. However, these are necessary conditions to obtain strong neutral lines. In fact, this model is constrained by the ratio of the O I/ C II line intensities. The observed O I lines are relatively strong and show that the emitting clumps should contain a large region of cool recombined gas (see §6).

In the last two columns of Table 2 the composite models SUM1 and SUM2 are listed. They result from the weighted sum of the contributions of the expanding shock (EXP)

spectrum and that emitted by the reverse shocks REV1 and REV2, respectively. The relative weights adopted are given in the bottom of Table 1. The fit presented in Table 2 is quite good, taking into account the disomogeneity of the emitting matter in the colliding region and the uncertainty of some atomic data in the code. The spectrum is so rich in number of lines that the fitting procedure constrains the model, thus providing the most probable description of the system. It seems that the best fit to the observed data is obtained by model SUM1.

The relative abundances calculated phenomenologically for models SUM1 and SUM2 are in agreement with those adopted in the model of Hayes & Nussbaumer (1986) within a factor of 2 (Table 1), except for Mg/H which is higher by a factor  $>20$ .

Model XX, which is also listed in Table 1, is characterized by a high  $V_s$  and a high  $n_0$  and will be discussed in the context of the continuum radiation in the next section. In fact, the full modeling of an object by the calculation of the emitted spectra implies the cross-checking of the results obtained for the line spectra with those obtained for the spectral energy distribution (SED) of the continuum. This procedure is necessary because it sometimes reveals that models other than those indicated by the fit of the line spectra must be taken into consideration.

#### 4.2. The continuum

Model calculations are compared with the observations in Fig. 4. The observed data are taken from Nussbaumer & Dumm (1997) in the wavelength range between 1280 and 2600 Å and from Kenyon et al (1986) in the IR. RR Tel has been detected as an X-ray source in 1978 by Einstein (Kwok & Leahy 1984) and in 1992 by ROSAT (Jordan, Murset, & Werner 1994). The data in the X-ray are taken from Fig. 3 of Kwok & Leahy (1984). The SED of the continua calculated by models REV1 and EXP are represented by solid lines and dotted lines, respectively. For each model besides the curve representing bremsstrahlung emission from the gas, reradiation by dust is represented by the curve in the IR ( $\nu < 10^{14}$  Hz). Generally, the temperature of the grains downstream follows the trend of the temperature of the gas (Viegas & Contini 1994, Fig. 3) therefore, the location of the dust reradiation peak depends on the shock velocity. On the other hand, the intensity of the dust radiation flux relative to bremsstrahlung emission depends on the dust-to-gas parameter, d/g.

The fit of model REV1 to the data in the IR yields to  $d/g = 5 \times 10^{-15}$ , whereas for model EXP to  $d/g = 10^{-14}$ . Since model EXP represents a shock front closer to the giant, a higher  $d/g$  implies a dustier atmosphere.

Fig. 4 shows that the radiation flux calculated by model REV1 strongly prevails on that calculated by EXP, and that some absorption is present in the low frequency domain.

As for the X-ray domain ( $10^{16} - 10^{18}$  Hz), the data show emission from a gas at a temperature between  $10^6$  and  $10^7$  K. Jordan et al. (1994) suggested that such a plasma could be produced by a fast wind with velocity of  $\sim 500 \text{ km s}^{-1}$ . This emission cannot be obtained either by the models which fit the emitting lines or by a black body spectrum corresponding to a colour temperature of  $1.4 \times 10^5$  K (dot-dashed line in Fig. 4). Actually, bremsstrahlung emission calculated by a model characterized by a high shock velocity (model XX in Table 1) nicely fits the data at higher frequencies (long dashed lines in Fig. 4). Notice that the point at  $\nu = 3 \times 10^{16}$  Hz is below the calculated curve since it is affected by absorption of the interstellar medium (ISM) (Zombeck 1990).

The high velocity model XX ( $V_s = 500 \text{ km s}^{-1}$ ) could explain the wide foot underneath the nebular emission of CIV, NV, and HeII lines observed by Nussbaumer & Dumm (1997). However, since large FWHM are not observed in the line profiles, the contribution of the spectrum calculated by the high velocity model to the line fluxes should be negligible. The line intensities calculated by model XX depend strongly on the geometrical thickness of the emitting clump ( $d$ ). To obtain line intensities lower than those from model REV1,  $d$  should be lower than  $6 \times 10^{13} \text{ cm}$ .

A high  $V_s$  is justified in a colliding scenario, as the wind collision yields to the disruption of the colliding matter and to the formations of clumps. The fast wind will propagate almost unaffected in the voids between the clumps.

An alternative scenario is represented by model X0 (short-dashed lines in Fig. 4) characterized by  $V_s = 500 \text{ km s}^{-1}$ , but with a lower density (about  $10^5 \text{ cm}^{-3}$ ). The downstream region at high temperature in the clumps is rather extended ( $> 5 \times 10^{14} \text{ cm}$ ) and leads to the emission which fits the high frequency data and to the requested almost negligible line fluxes.

### 4.3. Variability on short time scale

The photometric lightcurve of RR Tel in 1978 is characterized by large fluctuations in the visual band (see §2). Penston et al (1983) addressed this problem but could not conclude whether these variations are caused by line or by continuum variations. Actually, [Cl III] 5539, [OI] 5577, [FeVI] 5631, and [NII] 5755 are the strongest lines which enter the broad band visual filter.

In our model the shocks propagate throughout disrupted matter, heating and ionizing clumps of different geometrical width. We present in Fig. 5 the calculated flux of these lines and of the continuum as a function of the distance from the shock front for model REV1. This distance represents the geometrical width of the clumps since the models are matter bound. It can be seen that, particularly, between  $10^{13}$  and  $10^{14}$  cm the line flux increases with distance from the shock front more than the continuum. This is a critical range for the thickness of the clumps and within this range the line variability dominates the variability of the continuum in the light curve.

## 5. The spectra in 1993

We have calculated the spectra in 1993 in the frame of the scenario proposed in §2. The models which better fit the observations are given in Table 3 and the line ratios are compared with the observations in Tables 4a and 4b.

### 5.1. The UV spectrum

In the 1993 UV spectrum the high ionization lines dominate, and the OI and CII lines are still present, although weakened. Therefore, a region of gas emitting low ionization-level and neutral lines must still be present. This corresponds to a model with low  $V_s$ , low or even absent  $U$ , and a large zone of emitting gas at low temperature. Similar conditions were adopted to fit the 1978 spectrum (model EXP). In other words, the contribution of the expanding shock to the emitted spectrum is unavoidable. Notice that the flux intensity of CIV has decreased by a factor of  $> 2$  with respect to the 1978 flux. In Table 4a line intensities relative to CIV = 100 are listed together with the FWHM from ZSH and the

observed line ratios (columns 3 and 4). Two models for the reverse shock follow in columns 5 and 6, and three models representing the expanding shock are given in columns 7, 8, and 9. In the last three columns of Table 4a the composite models sum1, sum2, and sum3 (which better fit the observations) are presented. The relative weight of the single contribution in these models are listed in the bottom of Table 3.

The best fit to the 1993 high level line spectrum, even if rough, is obtained by model rev1 which is characterized by a high  $n_0$ . In particular, the calculated intensity of [MgVI] 1806 line increased by a factor of 1.9 from 1978. This trend agrees with the data listed by ZSH (Fig. 2). The other parameters of model rev1 (Table 3) suggest that, compared with 1978, the shock velocity has slightly decreased, the densities are higher, and  $U$  is lower than for model REV1 (see Table 1). A similar situation was found in the evolution of HM Sge (Formiggini et al 1995).

On the other hand, comparing the FWHM of the low ionization and neutral lines between 1978 and 1993, the expanding shock has maintained the same velocity, or even increased slightly. Three different models are considered, because, depending on the location of the shock front, the preshock density can be very different. We have adopted the same velocity for all the low level lines even if the FWHM of these lines (Table 4b) show a wide range of values from  $17 \text{ km s}^{-1}$  of [OI] 6300 to  $83 \text{ km s}^{-1}$  of [NII] 6584.

Model exp1 represents the case in which the shock front is still near the giant star (Fig. 3b) and a high density characterizes the preshocked gas. The expanding shock has maintained roughly the same velocity compared to that in 1978 (model REV in Table 1). In 15 years the shock could have overcome the red giant and be now propagating in the giant atmosphere on the side opposite to the WD, where the density gradient is decreasing. It is therefore predictable that radiation from the WD should be very low or even absent because of dilution and/or screening effects.

Two other models seem acceptable. In model exp2 the shock has reached a larger distance from the giant on the side opposite to the WD (Fig. 3b). At this distance, the density is lower and the shock velocity is higher because the shock accelerates while propagating through the decreasing density gradient in the giant atmosphere. The relative abundances are the same as those adopted for the other models because the shock is propagating within the system.

Model exp3 represents a different situation: the expanding shock colliding face-on-tail

with the wind from the giant reached the outskirts of the system (Fig. 3b) and is now propagating in the ISM characterized by a lower density. The relative abundances are close to the solar ones because mixing is rather strong at those large distances. In this model the shock could have traveled in about 15 years to a distance beyond  $2.3 \times 10^{15}$  cm. The geometrical thickness of the emitting slab is large. The radiation flux from the hot star is not prevented from reaching the inner edge of the slab but is low.

Notice that the three models exp1, exp2, and exp3 contribute only to low level lines in the UV spectrum which are few compared to the numerous high level lines. Therefore, we will constrain the models by the fit of the optical spectrum where the low level lines are as numerous as the high level ones. The consistent fit of line spectra in the different frequency ranges implies cross checking of one another until a fine tuning of all of them is found.

## 5.2. The spectrum in the optical range

In Table 4b observed line intensities in the optical range are compared with model calculations. These lines are those which are common to the observations of McKenna et al (1997) and the SUMA code. The lines in the optical range are given relative to  $H\beta = 1$ . For consistency, the same models used to fit the line in the UV are adopted. However, model rev2 is omitted.

Notice that [OII] 3727, even if low, is present in the spectra. Considering that [OII] has a critical density for collisional deexcitation  $\geq 3 \times 10^3$  cm $^{-3}$ , the density in the emitting gas cannot be much higher. The electron density downstream decreases with recombination (§6), therefore, even preshock densities higher than the critical one can fit the [OII]/  $H\beta$  line ratio. On this basis, model exp3 is more acceptable than exp1 and exp2.

The calculated [OIII] 4959+5007 is rather high compared with the observed line. A lower weight of model exp3 in the weighted sum (sum3) could improve the fit of [NII] 5754  $H\beta$  and [OIII]/  $H\beta$ , but definitively spoil the fit of [OII]/  $H\beta$ .

Interestingly, a low  $R_{[OIII]} = [OIII] 5007 / [OIII] 4363$  ratio coexists with a relatively high [OII] 3727 /  $H\beta$  ratio. Low  $R_{[OIII]}$  is generally due to either high density or high temperature of the emitting gas. High temperatures are excluded because the shock velocity is low. Therefore, high densities are indicated by  $R_{[OIII]}$  and low densities by [OII]/  $H\beta$ .

This peculiarity of the spectrum strengthens the hypothesis of a composite model. In fact, the low [OIII] 5007 / [OIII] 4363 ratio comes from the rev1 model while the relatively high [OII] 3727 / H $\beta$  ratio comes from model exp3. The [OI] 6300 / H $\beta$  line ratio, even if not very high, indicates that a large zone of neutral oxygen is present and is consistent with the large  $d$  ( $2 \times 10^{15}$  cm) of model exp3. The relatively high [OI]/ H $\beta$  line ratio appears also in model sum2 if a weight of 100 (see Table 3) is adopted for model exp2. This is rather high and definitively spoils the fit of most of the other line ratios. The composite model sum1 nicely fits most of the optical-near IR lines, however, [OI]/ H $\beta$  and [NII] 6584+ / H $\beta$  are largely overestimated.

In the composite model sum3, model exp3 has been given a weight three times that of model rev1. This is acceptable considering that the emission from the nebula between the components is certainly smaller than that from the nebula encircling the system.

Following the analysis of the optical spectrum, the composite model sum3 is selected. This model also fits the UV spectrum best, even if the OI 1304 / CIV line ratio is underestimated (Table 4a).

## 6. The RR Tel system in the epochs 1978 and 1993

After selecting the composite models which best fit the spectra observed in each of the epochs, a more quantitative description of the system can be given.

The results of model calculations give a rough physical picture of RR Tel in 1978. The distance  $r_{rs}$  of the reverse shock from the WD can be calculated from :

$$U n c = N_{ph} (R_{wd}/r_{rs})^2 \quad (1)$$

where  $N_{ph}$  is the Plank function corresponding to  $T_* = 1.4 \times 10^5$  K, and the WD radius  $R_{wd} = 10^9$  cm. Adopting the parameters of model REV1,  $N_{ph} = 3.4 \times 10^{26}$  photons  $\text{cm}^{-2} \text{s}^{-1}$ , and considering the density  $n = 4 n_0$  at the leading edge of the clumps due to the adiabatic jump,  $r_{rs} = 1.1 \times 10^{14}$  cm.

Applying equation (1) to the expanding shock (model EXP), the distance between the wd and the low velocity slab ( $r_{es}$ ) can be calculated. In this case the density  $n$  is given after compression downstream ( $n = 3.2 \times 10^7 \text{ cm}^{-3}$ ) and  $r_{es}$  results  $1.37 \times 10^{15}$  cm. The expanding shock is very close or even overpassing the red giant, considering the wide

interbinary separation ( $\sim 10^{15}$  cm).

In 1993 the reverse shock is at about the same distance from the wd as in 1978. On the other hand, from equation (1), the expanding shock represented by model exp3 has reached a distance of about  $5 \cdot 10^{15}$  cm corresponding to the outskirts of the system (§5.1)

As for the X-ray, the detection by ROSAT in 1992 (Jordan et al 1994) indicates that the high velocity wind ( $500 \text{ km s}^{-1}$ ) component is unchanged from 1978 (§4.2).

We compare now the physical conditions in the emitting gas at the two epochs.

The profiles of the fractional abundance of the most significant ions throughout the clumps in the two epochs are compared in Figs. 6a (1978) and 6b (1993). In both figures the WD is on the left. The diagrams on the left represent the clump downstream of the reverse shock and the diagrams on the right the clump downstream of the expanding shock. Notice that the black body radiation from the hot star reaches the very shock front edge in the reverse shocked clumps and the edge opposite to the shock front in the expanding ones. To better understand the physical conditions in the emitting regions the profiles of the electron temperature,  $T_e$ , and of the electron density,  $N_e$ , in a logarithmic scale are also given in the top of the figures.

First, we focus on models REV1 and rev1 (left side of Figs. 6a and 6b), the spectra of which largely prevail in the weighted sums of both epochs. It can be noticed that  $\text{He}^{+2}/\text{He}$  and  $\text{C}^{+4}/\text{C}$  are very high throughout the clump geometrical width. The dotted vertical lines in Figs. 6a and 6b show the actual geometrical thickness of matter bound models. For comparison the radiation bound model results are also shown beyond these lines. The observational data show that CIV and HeII line intensities prevail and that NV/CIV, HeII/CIV, and, - in a reduced way - also OV/CIV line ratios, increase from 1978 to 1993 (see Tables 2 and 4). In the same time CIV absolute flux decreases by a factor of  $> 2$ . The fit to these observations can be obtained by slightly reducing the shock velocity and the ionization parameter, and by increasing the preshock density, but, particularly, the geometrical thickness of the clump must be reduced by a factor larger than 2 (Tables 1 and 3).

Regarding the expanding shock, the physical conditions across the clumps in 1978 (model EXP) and 1993 (model exp3) are very different (Figures 6a and 6b diagrams on the right side of the figures). The clump is divided in two halves by the vertical solid line. The

x-axis scale is logarithmic and symmetric to have a comparable view of the two parts of the clump. The shock front is on the right while the edge photoionized by the WD radiation is on the left. In 1993 the electron density never exceeds  $10^5 \text{ cm}^{-3}$ . The region corresponding to the  $\text{O}^{+0}$  ion prevails in 1978 throughout the whole clump, while in 1993 is reduced to the shock dominated region.

## 7. Conclusions

In the previous sections we presented a model for RR Tel at two epochs. The first one (1978) is characterized by large fluctuations in the light curve and in the line intensities on very short time scales. In the second epoch (1993) the system recovered the fading trend. This epoch is considered with the aim of investigating the evolution of the system.

After the outburst, two shocks are present : the reverse shock propagates in the direction of the WD and the other one expands towards or beyond the giant. A good fit of the observed emission line spectra and continuum in 1978 is provided by a composite model, where the reverse shock is characterized by a velocity of  $\sim 80 \text{ km s}^{-1}$  and the expanding one by a velocity of  $\sim 45 \text{ km s}^{-1}$ . A high velocity ( $500 \text{ km s}^{-1}$ ) wind component is revealed from the fit of the SED of the continuum in the X-ray range in 1978, but it is quite unobservable in the line profiles if the geometrical thickness of the clumps is lower than  $6 \times 10^{13} \text{ cm}$ .

The large fluctuations observed in the 1978 light curve result from line intensity rather than from continuum variation. These variations are explained by fragmentation of matter at the time of head-on collision of the winds from the two stars.

The results of our modeling show that in 1993 the reverse shock velocity has slightly decreased ( $70 - 50 \text{ km s}^{-1}$ ) and the expanding shock with velocity between 50 to 100  $\text{km s}^{-1}$  has overcome the symbiotic system and is propagating in the nearby ISM. The decrease in the absolute flux of CIV is justified by the reduced shock velocity and ionization parameter. However, the geometrical thickness of the emitting clumps is the critical parameter which can explain the short time scale variabilities of the spectrum and the trend of slow line intensity decrease.

Relative abundances of carbon, nitrogen, oxygen, and silicon, to hydrogen, calculated by the present model, are in agreement with those assumed by the model of Hayes &

Nussbaumer (1986).

Finally, although our modeling is rather simplistic it shows that shock models can contribute to a better understanding of the outburst evolution of RR Tel.

#### Acknowledgements

We are grateful to an anonymous referee for helpful comments and to G. Drukier for reading the manuscript.

## References

Aller, L.H., Polidan, R.S., & Rhodes, E.J. 1973, *Ap&SS*, 20, 93

Aufdenberg, J.P. 1993 *ApJS* 87, 337

Bateson, F.M. 1995, private communication

Bohigas, J., Echevarria, J., Diego, F., Sarmiento, J. A., 1989, *MNRAS*, 238, 1395

Contini, M. 1997, *ApJ*, 483, 886

Feast, M.W. et al. 1983, *MNRAS*, 202, 951

Formiggini, L., Contini, M., Leibowitz, E.M. 1995, *MNRAS*, 277, 1071

Girard, T., Willson, L. A., 1987, *A&A*, 183, 247

Hayes, M.A. & Nussbaumer, H. 1986, *A&A*, 161, 287

Heck, A. & Manfroid, J. 1985, *A&A*, 142, 341

Jordan, S., Murset, U., & Werner, K. 1994, *A&A*, 283, 475

Kenyon, S.J., Fernandez-Castro, T., & Stencel, R.E. 1986, *AJ*, 92, 1118

Kenyon, S.J. et al 1993, *AJ*, 106, 1573

Kwok, S. & Leahy, D.A. 1984, *ApJ*, 283, 675

McKenna, F. C. et al. 1997, *ApJS*, 109, 225

Murset, U., Nussbaumer, H., Schmid, H.M., & Vogel, M. 1991, *A&A*, 248, 458

Nussbaumer, H. & Dumm, T. 1997, *A&A*, 323, 387

Nussbaumer, H., & Schild, H. 1981, *A&A*, 101, 118

Nussbaumer, H., Walder, R., 1993, *A&A*, 278, 209

Penston, M.V. et al. 1983, *MNRAS*, 202, 833

Thackeray, A.D. 1977, MNRAS, 83, 1

Viegas, S. M., Contini, M., 1994, ApJ, 428, 113

Viotti, R. 1988 in "The Symbiotic Phoenomenon" eds. J.Mikolajewska et al. Kluwer Academic Publishers, p. 269

Wallerstein, G., Willson, L. A., Salzer, J., Brugel, E., 1984, A&A, 133, 137

Withelock, P.A. 1988 in "The Symbiotic Phoenomenon" eds. J.Mikolajewska et al. Kluwer Academic Publishers, p. 47

Zombeck, M.V. 1990 in "Handbook of Space Astronomy and Astrophysics" Cambridge University Press, p. 199

Zuccolo, R., Selvelli, P., & Hack, M. 1997, A&AS, 124, 425 (ZSH)

## Figure Captions

Fig.1 :

The light curve of RR Tel between the years 1944 and 1993.

Fig. 2 :

The evolution of some significant line intensities between 1978 and 1993. from ZSH Table 1. Saturated fluxes are arbitrarily set at  $\log(I) = 2$ .

Figs. 3 :

Simple sketch of the model for RR Tel in 1978 and in 1993. The asterisk indicates the WD and the full circle the cool giant. Shock fronts are indicated by solid lines. Dotted and long-dashed lines indicate the clump edge opposite to the shock front. Dashed arrows represents the radiation from the WD. a) 1978; b) 1993

Fig. 4 :

The SED of the continuum in the year 1978. Full squares represent the observations and the curves represent model calculations (see text).

Fig. 5 :

The intensity of some lines in the visual band calculated as a function of the distance from the shock front.

Figs. 6 :

The distribution of the ions corresponding to the strongest line throughout the clumps (see text). a) 1978, b) 1993.

Table 1  
The parameters of Table 2

---

	REV1	REV2	EXP	XX	HN(1986)
$V_s$ (km s $^{-1}$ )	80.	85.	45.	500	-
$n_0$ (cm $^{-3}$ )	1(6)	1(5)	2(6)	1(6)	-
$B_0$ (gauss)	1(-3)	1(-3)	1(-3)	1(-3)	-
$T_*$ (K)	1.4(5)	1.4(5)	1.4(5)	1.4(5)	2.(5)
U	0.2	0.2	2.(-4)	0.2	-
d (cm)	5.5(13)	8.15(14)	1.(14)	< 5.9(13)	-
d/g	1(-14)	5(-15)	1(-14)	5(-15)	-
CIV (erg cm $^{-2}$ s $^{-1}$ )	9.4(3)	1.(3)	5.9(-4)	<0.016	-
He/H	0.1	-	0.1	-	0.2
C/H	3.3(-4)	-	3.3(-4)	-	3.5(-4)
N/H	5.4(-4)	-	5.4(-4)	-	3.(-4)
O/H	8.6(-4)	-	8.6(-4)	-	9.(-4)
Mg/H	6.9(-4)	-	6.9(-4)	-	3.(-5)
Si/H	5.3(-5)	-	5.3(-5)	-	3(-5)
W (SUM1)	1.	-	1.	-	-
W (SUM2)	-	1.	1.	-	-

---

Table 2  
line ratios to CIV = 100 (1978)

	line	FWHM	obs.	REV1	REV2	EXP	SUM1	SUM2
		km s <sup>-1</sup>	ZSH					
1199	[SV]	47.	1.51?	0.45	0.4	-	0.45	0.4
1206	SiIII	55.	1.15	1.2	0.85	4.9(5)	1.2	1.14
1218	OV]	59.	9.63	9.6	9.6	-	9.6	9.6
1236	NV	61	27.14	31.	32.	-	31.	32.
1242	NV	51.	13.67	-	-	-	-	-
1264	SiII	45.	0.08	0.016	0.01	3.1(6)	0.2	1.8
1302	OI	51.	1.41	-	-	3.7(6)	0.23	2.2
1305	OI	39.	0.30	↑	↑	↑	↑	↑
1306	OI	48.	2.16	↑	↑	↑	↑	↑
1324	[MgV]	72.	0.33	0.3	0.3	-	0.3	0.3
1334	CII	40.	0.29	0.07	0.12	1.8(5)	0.1	0.23
1335	CII	65.	0.45	0.03	0.02	7(6)	0.45	4.1
1393	SiIV	49.	6.64b	11.	10.	-	11.	10.
1398	SIV]	43	-	0.3	0.28	-	0.3	0.28
1401	OIV]	47.	8.37b	7.8	6.9	1.1(4)	7.8	6.9
1404	OIV]+ SIV]	47.	4.73b	4.6	4.0	-	4.7	4.0
1407	OIV]	53.	1.34	1.2	1.2	-	1.2	1.2
1483	NIV]	49.	0.41	0.56	0.5	-	0.56	0.5
1486	NIV]	42.	9.49b	43	37.	-	43.	37.
1533	SiII	66.	0.24	0.012	.012	7(5)	0.06	0.42
1548	CIV	52.	66.55a	100	100	100	100	100
1551	CIV	50.	34.40a	↑	↑	↑	↑	↑

	line	FWHM	obs.	REV1	REV2	EXP	SUM1	SUM2
		km s <sup>-1</sup>	ZSH					
1574	[NeV]	61.	2.95	0.17	0.11	-	0.17	0.11
1601	[NeIV]	64.	1.88b	2.3	2.3	-	2.3	2.3
1640	HeII	71.	30.70	32	36.	1.6(7)	32.	45.
1660	OIII]	38.	2.57b	5.1	6.8	-	5.1	6.8
1666	OIII]	36.	7.61	↑	↑	↑	↑	↑
1718	NIV	78.	0.27	0.25	-	-	0.25	-
1746	NIII]	48.	0.12	↓	↓	↓	↓	↓
1748	NIII]	45.	0.43	↓	↓	↓	↓	↓
1749	NIII]	41.	1.77b	4.2	8.	1.2(4)	4.2	8.
1752	NIII]	48.	0.72b	↑	↑	↑	↑	↑
1754	NIII]	44.	0.37b	↑	↑	↑	↑	↑
1806	[MgVI]	-	-	0.3	0.9	-	0.3	0.9
1808	SiII	45.	0.36	0.05	0.07	2.1(6)	0.18	1.3
1814	[NeIII]	43.	0.19	0.07	0.07	1.8(4)	0.08	0.07
1882	SiIII	-	0.04	↓	↓	↓	↓	↓
1892	SiIII	40.	5.10a	6.6	5.5	1.5(6)	6.7	6.4

Table 3  
The parameters of Tables 4a and 4b

	rev1	rev2	exp1	exp2	exp3
$V_s$ (km s $^{-1}$ )	60.	70.	50.	100.	50.
$n_0$ (cm $^{-3}$ )	2(6)	2(5)	5(6)	3(5)	2(4)
$B_0$ (gauss)	1(-3)	1(-3)	1(-3)	1(-3)	1(-3)
$T_*$ (K)	1.4(5)	1.4(5)	1.4(5)	1.4(5)	1.4(5)
U	0.1	0.1	0.	0.	5(-3)
d (cm)	2.9(13)	6.(12)	> 8.8(13)	1.7(13)	2(15)
d/g	1(-14)	1(-14)	1(-14)	1(-14)	1(-14)
CIV (erg cm $^{-2}$ s $^{-1}$ )	4.4(3)	440.	3.(-4)	12.	0.09
$H\beta$ (erg cm $^{-2}$ s $^{-1}$ )	204.		139.	0.12	0.84
C/H	3.3(-4)		3.3(-4)	3.3(-4)	3.3(-4)
N/H	5.4(-4)		5.4(-4)	5.4(-4)	1.4(-4)
O/H	8.6(-4)		8.6(-4)	8.6(-4)	6.6(-4)
Mg/H	6.9(-4)		6.9(-4)	6.9(-4)	6.9(-4)
Si/H	5.3(-5)		5.3(-5)	5.3(-5)	5.3(-5)
W (sum1)	1.	-	1.	-	-
W (sum2)	1.	-	-	100.	-
W (sum3)	1.	-	-	-	3.

Table 4a

### UV line ratios to CIV = 100 (1993)

---

	line	FWHM	obs.	rev1	rev2	exp1	exp2	exp3	sum1	sum2	sum3
		km s <sup>-1</sup>	ZSH								
1574	[NeV]	55.	5.4	0.3	0.19	-	2(-3)	-	0.3	0.23	0.3
1601	[NeIV]	56.	3.09	3.3	2.7	-	0.9	-	3.3	2.8	3.3
1640	HeII	66.	51.3	40.	34.	10.	0.24	-	40.	31.5	40.
1660	OIII]	41.	3.26	3.3	4.8	1.3(4)	21.2	167.	3.3	7.13	3.3
1666	OIII]	38.a	9.44a	-	-	-	-	-	-	-	-
1746	NIII]	81.	0.13	↓	↓	↓	↓	↓	↓	↓	↓
1748	NIII]	39.	0.49	↓	↓	↓	↓	↓	↓	↓	↓
1749	NIII]	41.	2.8	3.	5.	4.7(5)	22.7	32.4	3.	7.22	3.
1752	NIII]	46.	1.1	↑	↑	↑	↑	↑	↑	↑	↑
1754	NIII]	34.	0.42	↑	↑	↑	↑	↑	↑	↑	↑
1806	[MgVI]	0.64	3.47	1.2	1.5	-	-	-	1.2	0.9	1.2
1808	SiII	65.	0.29	0.06	0.13	2.9(7)	1.45	210.	2.	0.36	0.07
1814	[NeIII]	33.	0.26	0.05	0.07	-	0.2	-	0.05	0.08	0.05
1882	SiIII	-	-	↓	↓	↓	↓	↓	↓	↓	↓
1892	SiIII	-	-	14.	1.5 (7)	44.7	15.	877.	14.	14.2	14.

---

Table 4b  
optical line ratios to H $\beta$  = 1. (1993)

	line	FWHM	obs	rev1	exp1	exp2	exp3	sum1	sum2	sum3
3710	SIII	50.	3.4(-3)	9.(-4)	7.(-4)	0.26	1.2(-3)	8.2(-4)	0.015	0.001
3729b+	[OII]	48.	0.02	-	2(-3)	0.22	1.2	8.2(-4)	0.012	0.014
3759	FeVII	69.	0.91	0.84	-	2.7(-3)	-	0.5	0.79	0.84
3869b+	[NeIII]	43.	0.79	0.4	-	3.1	2.5	0.23	0.55	0.42
4068+	[SII]	46.	0.02	-	0.33	0.6	1.7	0.13	0.03	0.02
4114	[FeII]	32.	4.9(-3)	-	0.19	0.16	0.36	0.08	8.8(-3)	4.3(-3)
4363	[OIII]	40.	0.5	0.54	-	5.	0.16	0.32	0.85	0.54
4625	[ArV]	45.	5.(-3)	0.019	-	3.(-3)	-	0.01	0.018	0.019
4686	HeII	57.	0.9	1.0	-	0.02	0.37	0.6	0.94	0.99
4740	[ArIV]	67.	0.013	7.2(-3)	-	6.(-3)	-	4.2(-3)	7.1(-3)	7.(-3)
4893	[FeVII]	65.	0.05	0.12	-	-	-	0.07	0.11	0.12
4959+	[OIII]	59.	0.35	0.6	-	11.	17.2	0.35	0.29	0.53
5676	[FeVI]	60.	1.4(-3)	0.06	-	0.09	-	0.03	0.06	0.06
5754	[NII]	41.	1.6(-3)	2.3(-3)	0.12	5.5	-	1.4(-3)	0.3	0.06
5876	HeI	41.	9.(-3)	7.4(-3)	7.(-3)	0.3	0.13	7.2(-3)	0.02	9.(-3)
6300+	[OI]	17.	9.(-3)	-	1.65	0.13	0.67	0.7	7.2(-3)	8.(-3)
6310+	[SIII]	40.	1.3(-3)	1.5(-3)	1.1(-3)	0.42	1.8(-3)	1.3(-3)	0.024	1.5(-3)
6584+	[NII]	83.	5.(-3)	4.(-4)	0.54	1.44	3.8	0.2	0.08	0.01

Fig. 1

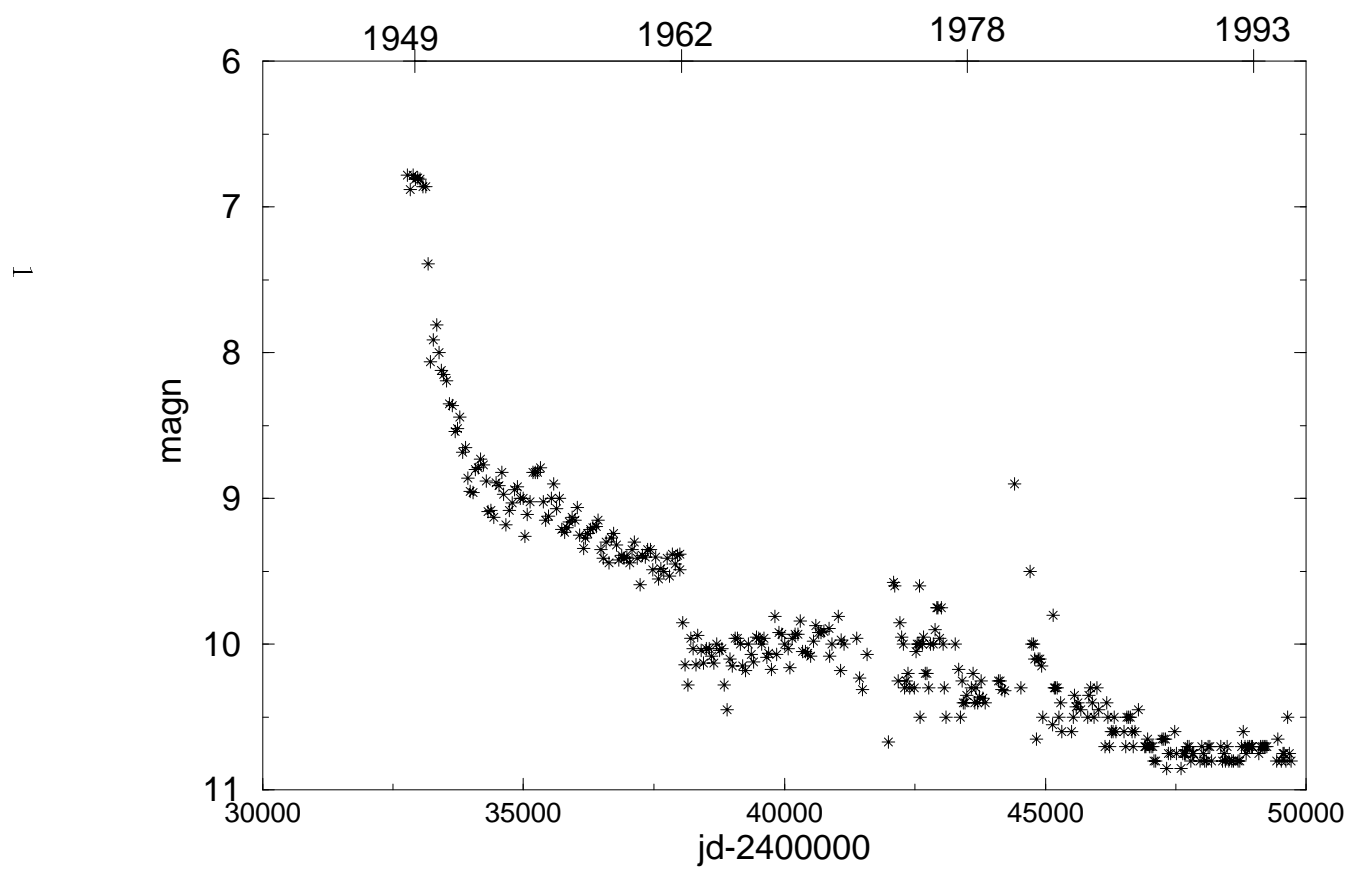


Fig. 2

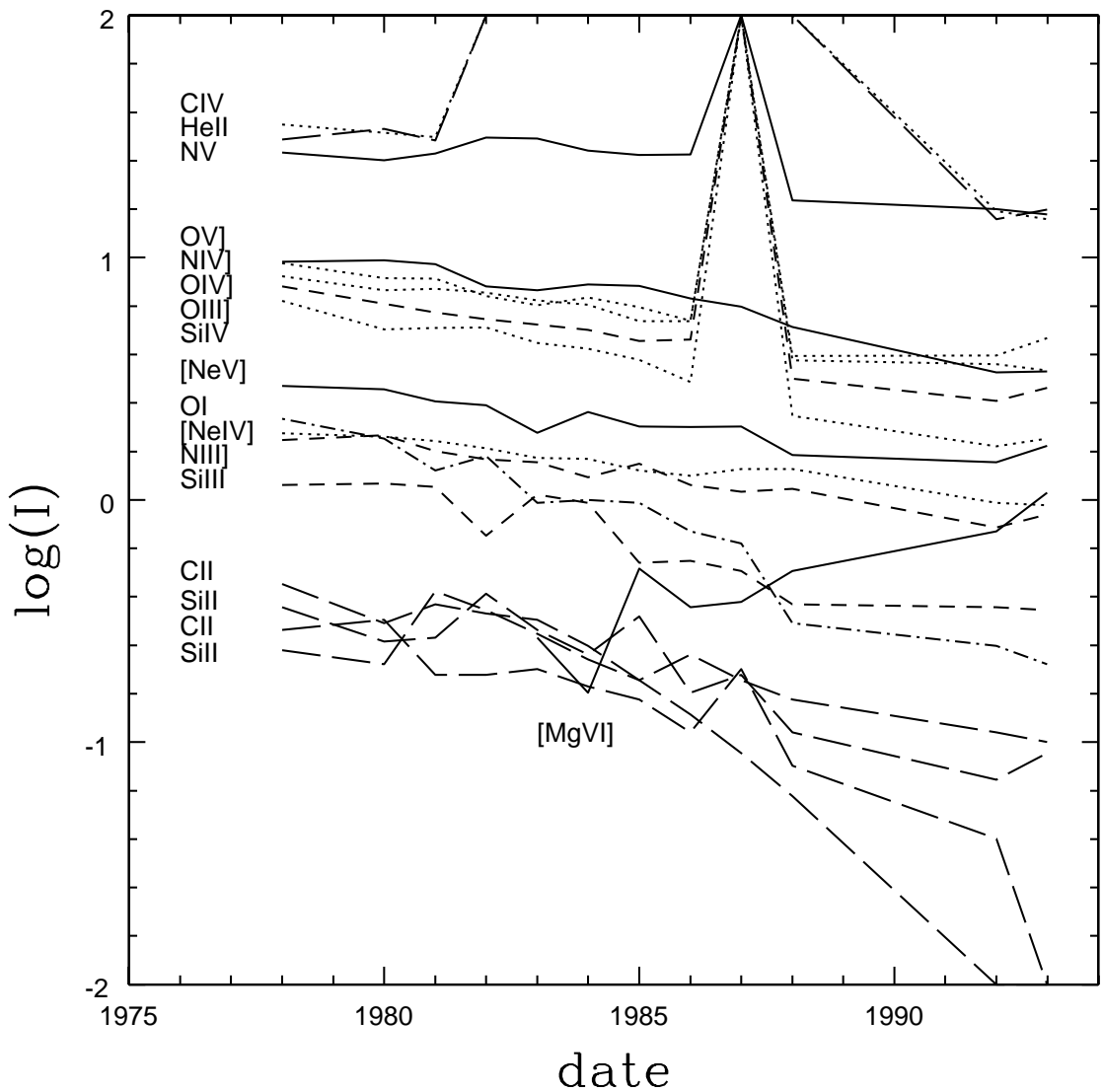


Fig. 3a

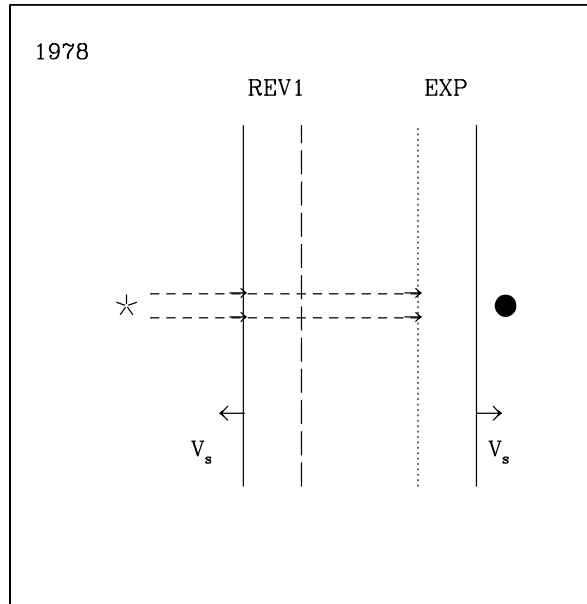


Fig. 3b

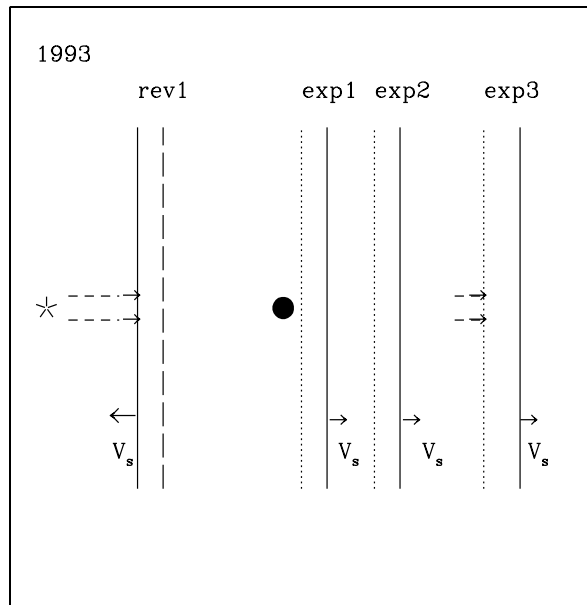


Fig. 4

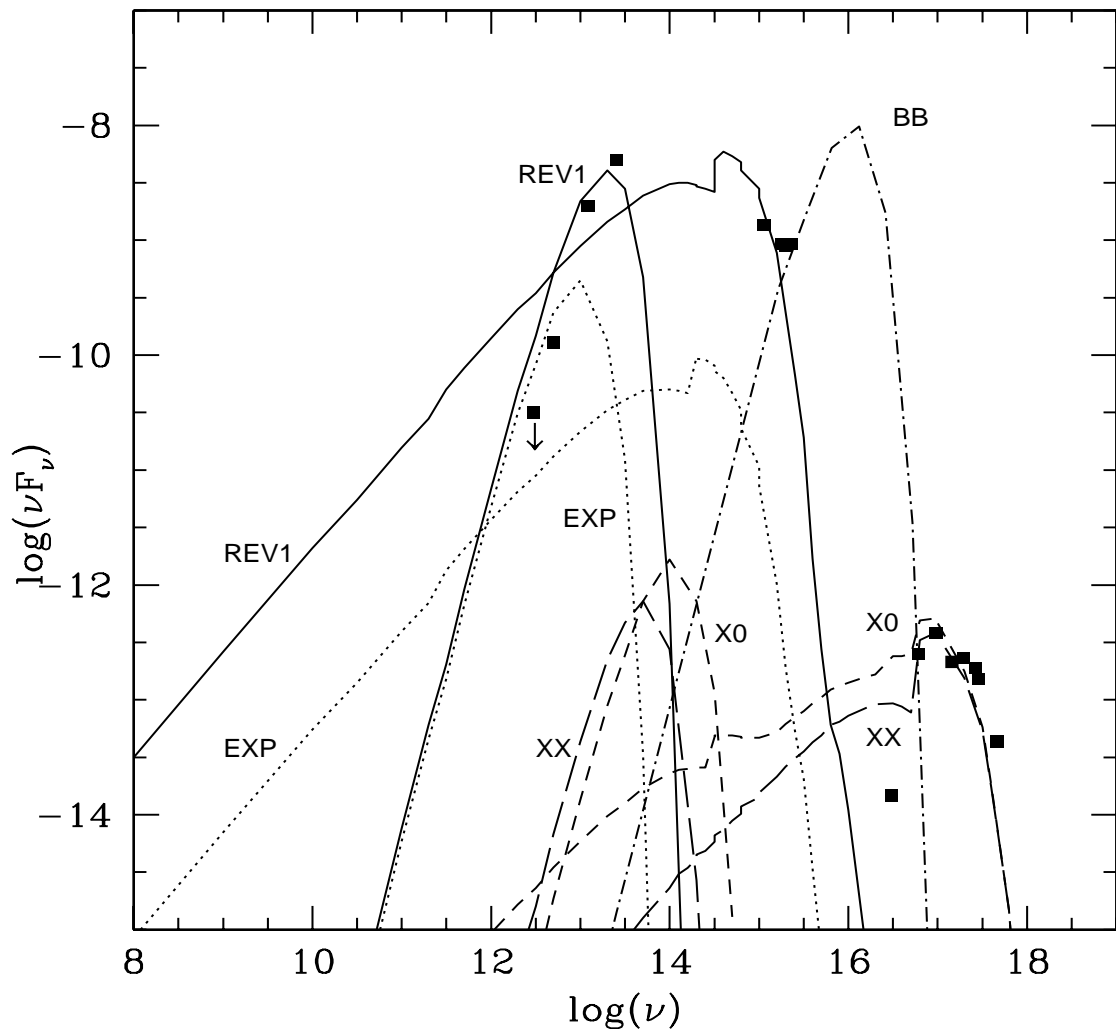


Fig. 5

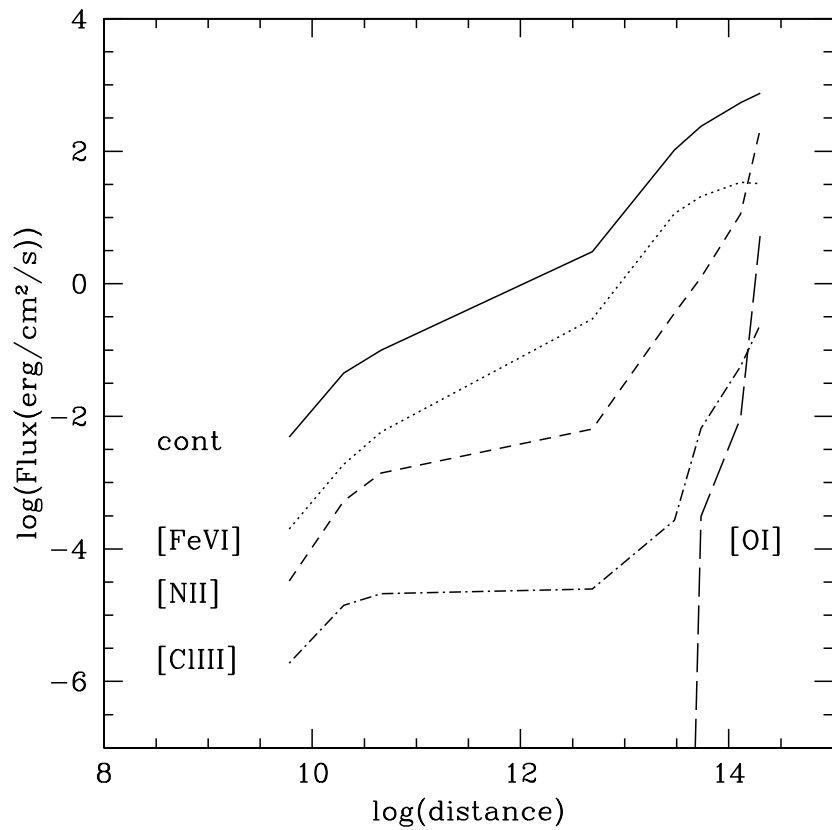


Fig. 6a

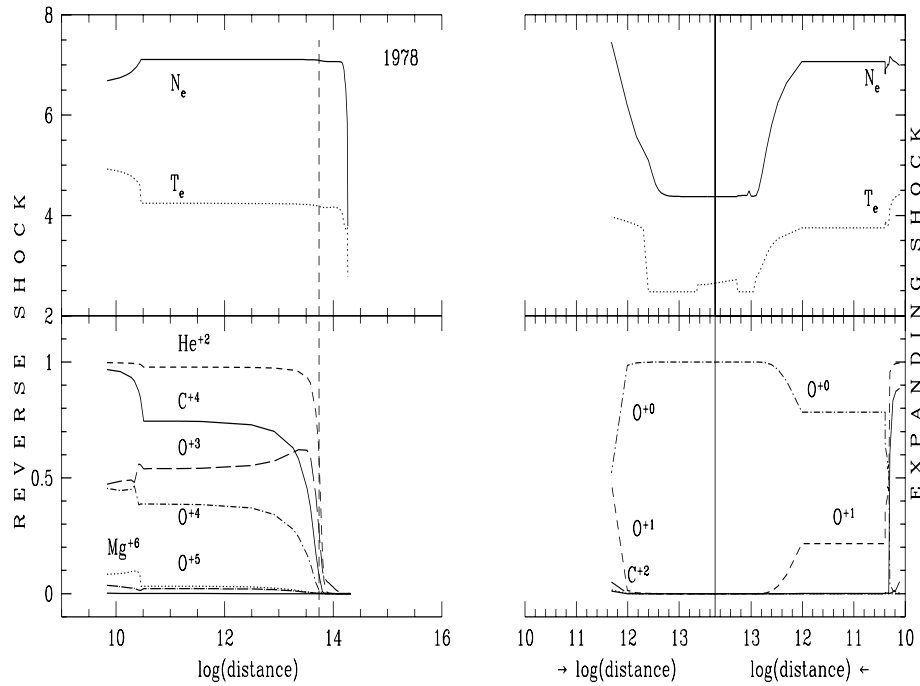


Fig. 6b

